STRUCTURAL SCIENCE
CRYSTAL ENGINEERING
MATERIALS

Volume 75 (2019)

Supporting information for article:

The structures and phase transitions in 4-aminopyridinium tetra-aquabis(sulfato)iron(III), (C5H7N2)[Fe^{III}(H2O)4(SO4)2]

Tamara J. Bednarchuk, Wolfgang Hornfeck, Vasyl Kinzhybalo, Zhengyang Zhou, Michal Dušek and Adam Pietraszko

Supporting information

Heat capacity was measured using Mettler Toledo DSC – 1 calorimeter with high resolution of 0.4 μW. Nitrogen was used as a purging gas and the heating and cooling rate was 5 K/ min. The sample mass was 26.60mg.

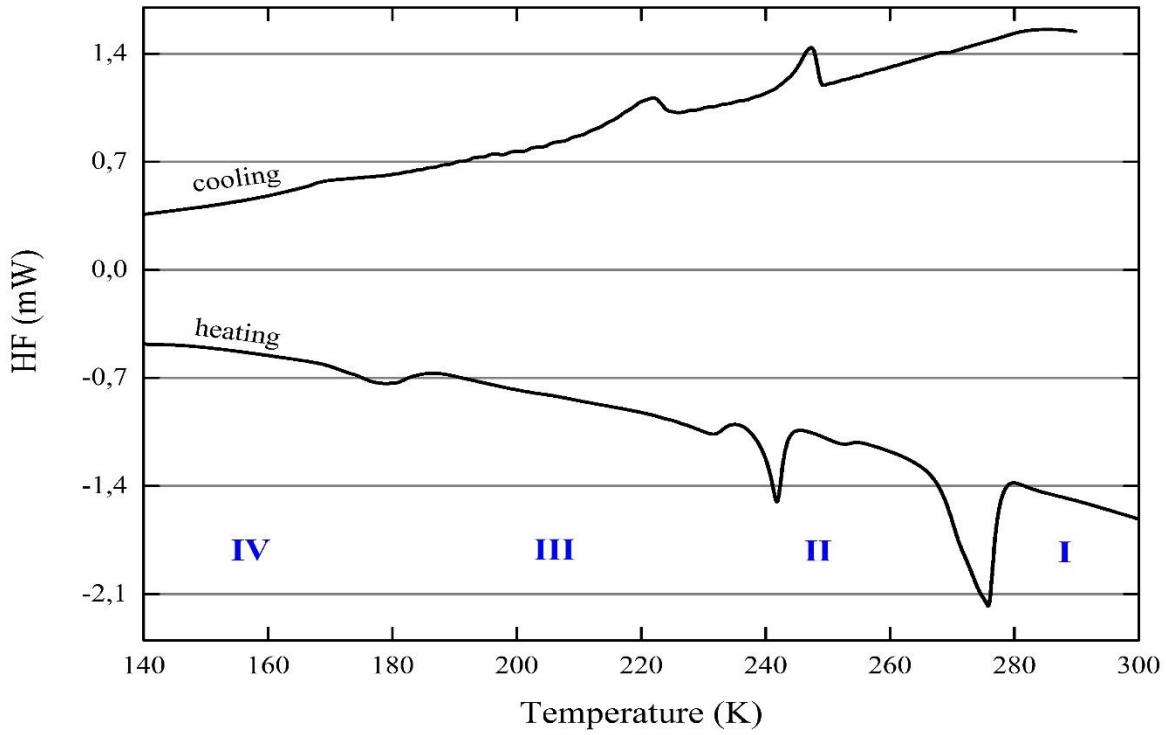

Figure S1 DSC curves for the title compound

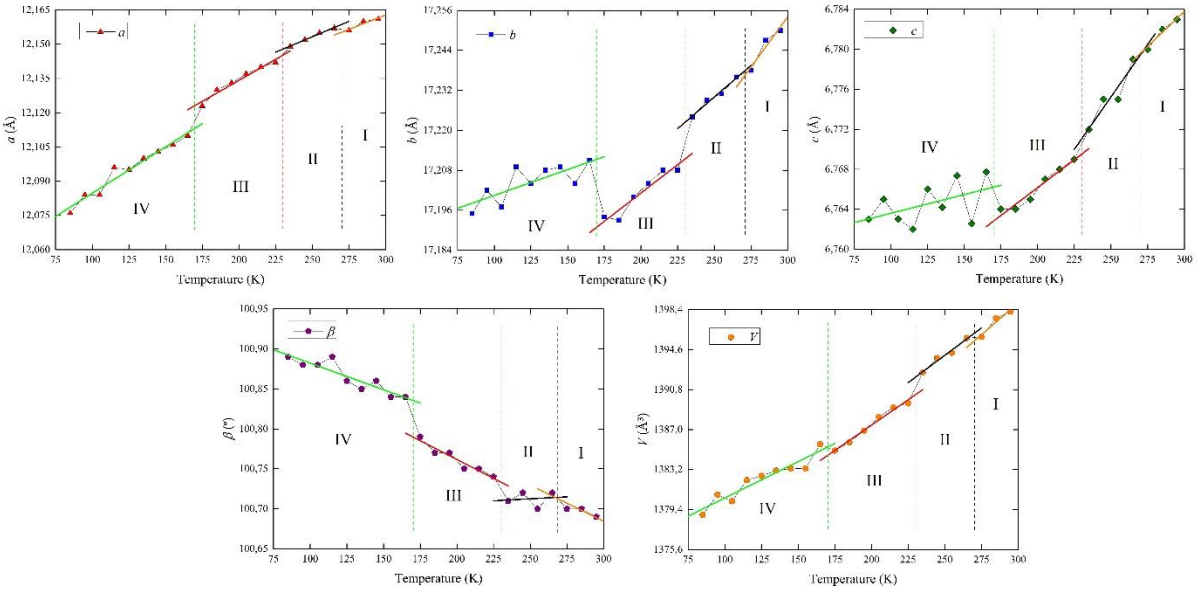

Figure S2 Temperature dependence of the lattice parameters *a*, *b*, *c*, *β* and the unit cell volume of 4-aminopyridinium tetraaquabis(sulfato)iron(III) for the cooling cycles from diffraction measurements. Dash vertical lines correspond to the structural phase transition determined from DSC.

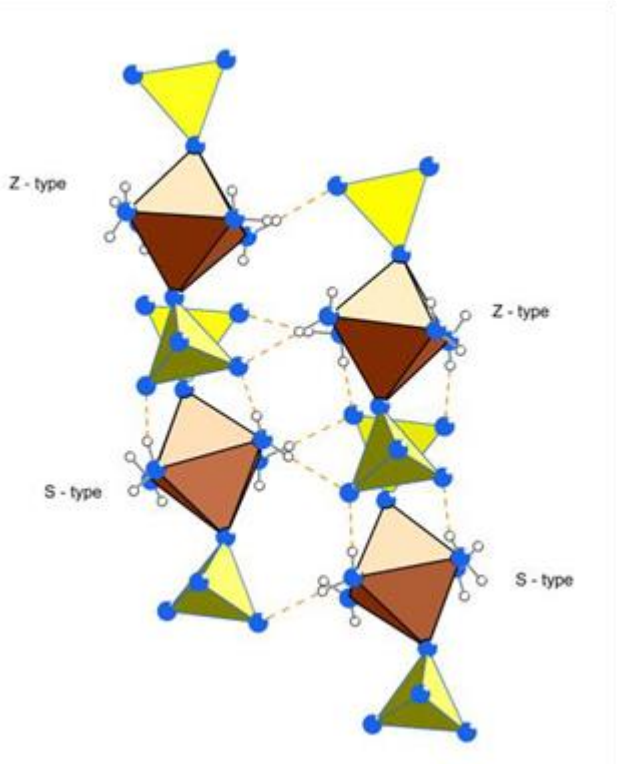

Figure S3 Alternating tilts of $[Fe^{III}(H_2O)_4(SO_4)_2]^-$complex anions forming hydrogen bonded double columns in the crystal structure of phase (IV).

S1. Other information

S1.1

Moreover, a CSD database search (version 5.38, November 2016) for sulfate anions bonded to iron (including free, terminal and μ2/μ3 bridging bonding modes) yielded 14 entries with a total of 20 sulfate anions considered, which show a similar flexibility in their bond lengths and angles distribution (1.437 Å to 1.587 Å; 103.37° to 114.72°). The bond valence sum for this selected set of cases varies from 5.86 to 6.21 valence units, i.e. within a similar range like the variation observed for the modulated case. Thus, the non-rigidity of the sulfate anion is a true chemical observation and neither a problem regarding the technicalities of the data acquisition/reduction nor a fault of the structure refinement, respectively.

S1.2

The Fe octahedra also show some non-rigidity, yet less pronounced than for the sulfate case (Figs. 5, 6). Clearly showing the expected oxidation state of +3, the bond valence sum variation for iron is

negligible (not shown). However, despite the complex variation of the angles, precluding a detailed understanding of the structural variations enforced by the modulation, the overall impression allows to clearly distinguish both modulated phases ((II) and (III)) from another, which shows more pronounced differences than for the sulfate case. While only two points of discontinuity are observed for phase (II), with the curves for related angles still approaching the discontinuity for the same limiting angle value, the situation found for phase (III) is much more complicated, exhibiting four points of discontinuity including jumps in the limiting values for the curve branches of related angles (Figure 6). While the observed differences are difficult to translate into an easily understandable chemical picture, they make a point in case of the observed transition between the modulated phases.

Finally, the part of the crystal structure least affected by the modulation is the 4ap cation. Taking the distance of the barycenters of the aromatic ring as an approximate measure of π–π stacking, one does observe only a small variation about 4.4 Å (not shown), which agrees well with the situation found in the non-modulated phases, the difference being caused by the non-perpendicular distance definition.

Another check for the soundness of the developed structure model is given by a simulation of its diffraction pattern. Usually the use of discontinous crenel functions leads to the presence of higher order satellites (as modelling block wave crenel functions with harmonic waves would require higher order contributions, too, with a direct correspondence existing between the order of the harmonic functions needed in the refinement and the satellites observed). However, the notable absence of satellite orders higher than one, as simulated for our model, matches the experimental observations, thereby featuring an exceptional case.

S1.3

The crystal in phase (IV) was treated as a two-component twin of triclinic cells related to each other by ~180° rotation around monoclinic *b** axis (transformation matrix, *mC* → *aP*, -½ ½ 0 ½ ½ 1 ½ ½ -1). The structure of phase (IV) was solved by direct methods from non-overlapped part of the reflections and refined by a full-matrix least-squares method on all F^2 data using the SHELX-2014 crystallographic software package [Sheldrick, G. M. (2015). Acta Cryst. C71, 3-8] *via* the Olex2 interface [Dolomanov, O. V., Bourhis, L. J., Gildea, R. J. & Howard, J. A. K. (2009). Appl. Cryst. 42, 339-341] using HKLF type 5 reflection file produced by CrysAlis data reduction program. Twin parameter was refined and was close to 50:50 twin ratio in all temperature range of phase (IV). All non-hydrogen atoms were refined with anisotropic temperature factors. The position of hydrogen atoms of the amines were initially located in the difference Fourier maps, and for the final refinement, the hydrogen atoms were placed geometrically. The hydrogen atoms of the water molecules were located from difference Fourier maps and were refined with O-H distances equal to 0.84 Å and *U*iso(H) = 1.5 *U*eq(O). ISOR instruction was use for restraining the anisotropic displacement parameters of N11 and N21 atoms (the effective standard deviation equal to 0.002).